Intramolecular C−H Bond Activation and Redox Isomerization across Two-Electron Mixed Valence Diiridium Cores

Arthur J. Esswein,[§] Adam S. Veige,[‡] Paula M. B. Piccoli,[†] Arthur J. Schultz,[†] and Daniel G. Nocera*,[§]

Department of Chemistry, 6-335, Massachusetts Institute of Technology, 77 Massachusetts Avenue, Cambridge, Massachusetts 02139-4307, and the Intense Pulsed Neutron Source, Argonne National Laboratory, Argonne, Illinois 60439-4814

Received July 30, 2007

Metal−metal cooperativity enables the reaction of carbon-based substrates at diiridium two-electron mixed valence centers. Arylation of $Ir_2^{0,II}(tfepma)_3Cl_2$ (**1**) (tfepma = bis[(bistrifluoroethoxy)phosphino]methylamine) with RMgBr (R = C_6H_5 and C_6D_5) is followed by C−H bond activation to furnish the bridging benzyne complex $Ir_2^{II,II}(tfepma)_3(\mu\text{-}C_6H_4)(C_6H_5)H$ (**2**), as the kinetic product. At ambient temperature, **2** isomerizes to $Ir_2^{I,III}(tfepma)_3(\mu\text{-}C_6H_4)(C_6H_5)H$ (**3**) ($k_{obs} = 9.57 \pm 0.10 \times 10^{-5}$ s^{-1} at 31.8 °C, $\Delta H^{\ddagger} = 21.7 \pm 0.3$ kcal/mol, $\Delta S^{\ddagger} = -7.4 \pm 0.9$ eu), in which the benzyne moiety is conserved and the Ir^{III} center is ligated by terminal hydride and phenyl groups. The same reaction course is observed for arylation of **1** with C_6D_5MgBr to produce **2**-d_{10} and **3**-d_{10} accompanied by an inverse isotope effect, $k_h/k_d = 0.44$ ($k_{obs} = 2.17 \pm 0.10 \times 10^{-4}$ s^{-1} in C_6D_6 solution at 31.8 °C, $\Delta H^{\ddagger} = 24.9 \pm 0.7$ kcal/mol, $\Delta S^{\ddagger} = -6.4 \pm 2.4$ eu). **2** reacts swiftly with hydrogen to provide $Ir_2^{II,II}(tfepma)_3H_4$ as both the *syn* and *anti* isomers (**4**-*syn* and **4**-*anti*, respectively). The hydrides of **4**-*syn* were directly located by neutron diffraction analysis. X-ray crystallographic examination of **2**, **2**-d_{10}, **3**, and **4**-*syn* indicates that cooperative reactivity at the bimetallic diiridium core is facilitated by the ability of the two-electron mixed valence framework to accommodate the oxidation state changes and ligand rearrangements attendant to the reaction of the substrate.

Introduction

Cooperative reactivity at a metal−metal core is based on the elementary premise that affixed metal centers working in concert will effect chemistry otherwise unattainable to mononuclear complexes.[1–6] For instance, some metal acyls, alkyls, and dihydrides are particularly sluggish toward intramolecular elimination, but become extremely unstable in the presence of a second metal complex. The enhanced reactivity has been ascribed to the following transformation (R = hydride, alkyl, or acyl).[7–9]

(1)

Dissociation of a ligand opens a coordination site to permit attack by a coordinatively saturated partner. Migration of the hydride into a position bridging the two metal centers produces the preferred transition state from which elimination may proceed smoothly. Owing to the bimolecular order of the above transformation, reactions proceeding through this dinuclear elimination-type transition state should be greatly enhanced if supported intramolecularly within a bimetallic core. We have shown this to be the case with two-electron mixed valence complexes, M^n-M^{n+2} (M = Rh, Ir), that are coordinated by bis(difluorophosphino)methylamine (dfpma, $CH_3N(PF_2)_2$) and bis[(bistrifluoroethoxy)phosphino]methylamine (tfepma, $CH_3N[P(OCH_2CF_3)_2]_2$) ligands. The ability of the bimetallic core to accommodate the electronic and steric asymmetries associated with oxidation state changes and ligand rearrangements is essential to the reactivity of two-electron mixed valence M^n-M^{n+2} complexes.[10] For the case of H_2 activation, computational studies show that the internal asymmetry of the two-electron mixed valence core is preserved as hydrogen is shuttled from one metal to the other through a critical bridging intermediate.[11]

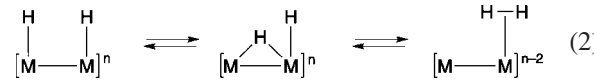

(2)

Atom shuttling through the bridging position of the bimetallic core has also been important to the activation, in two-electron steps, of other small molecules such as HX ($X = Cl^-$, Br^-),[12]

* Corresponding author. E-mail: nocera@mit.edu.
§ Massachusetts Institute of Technology.
‡ Current address: Department of Chemistry, University of Florida, P.O. Box 117200, Gainesville, FL 32611-7200.
† Argonne National Laboratory.

(1) Bosnich, B. *Inorg. Chem.* **1999**, *38*, 2554–2562.
(2) McCollum, D. G.; Bosnich, B. *Inorg. Chim. Acta* **1998**, *270*, 13–19.
(3) Gavrilova, A. L.; Bosnich, B. *Chem. Rev.* **2004**, *104*, 349–384.
(4) Fackler, J. P. Jr. *Inorg. Chem.* **2002**, *41*, 6959–6972.
(5) Adams, R. D.; Captain, B.; Zhu, L. *J. Am. Chem. Soc.* **2006**, *128*, 13672–13673.
(6) Adams, R. D.; Captain, B.; Zhu, L. *J. Am. Chem. Soc.* **2007**, *129*, 7545–7556.
(7) Norton, J. R. *Acc. Chem. Res.* **1979**, *12*, 139–145.
(8) Martin, B. D.; Warner, K. E.; Norton, J. E. *J. Am. Chem. Soc.* **1986**, *108*, 33–39.
(9) Kristjánsdóttir, S. S.; Norton, J. A. In *Transition Metal Hydrides*; Dedieu, A., Ed.; VCH: New York, 1990; Chapter 9.
(10) Gray, T. G.; Veige, A. S.; Nocera, D. G. *J. Am. Chem. Soc.* **2004**, *126*, 9760–9768.
(11) Veige, A. S.; Gray, T. G.; Nocera, D. G. *Inorg. Chem.* **2005**, *44*, 17–26.
(12) Heyduk, A. F.; Nocera, D. G. *Science* **2001**, *293*, 1639–1641.

10.1021/om7007748 CCC: $40.75
Publication on Web 02/20/2008

Table 1. Crystallographic Summary for Complexes 2−4-*syn*

	2·(CH_2Cl_2)	**2**-d_{10}·(CH_2Cl_2)	**3**	**4**-*syn* (X-ray)	**4**-*syn* (neutron)
formula	$C_{40}H_{45}F_{36}Ir_2N_3O_{12}P_6Cl_2$	$C_{40}H_{35}D_{10}F_{36}Ir_2N_3O_{12}P_6Cl_2$	$C_{39}H_{43}F_{36}Ir_2N_3O_{12}P_6$	$C_{27}H_{37}F_{36}Ir_2N_3O_{12}P_6$	$C_{27}H_{37}F_{36}Ir_2N_3O_{12}P_6$
fw, g/mol	2084.91	2094.91	1999.98	1849.82	1849.82
cryst syst	triclinic	triclinic	monoclinic	triclinic	triclinic
space group	$P\bar{1}$	$P\bar{1}$	$P2_1/c$	$P\bar{1}$	$P\bar{1}$
color	colorless	colorless	colorless	colorless	colorless
cryst dimens, mm	0.20 × 0.12 × 0.10	0.25 × 0.20 × 0.10	0.12 × 0.10 × 0.06	0.25 × 0.25 × 0.20	2 × 2 × 1
a, Å	12.975(2)	12.957(2)	21.1423(13)	12.0419(6)	11.982(4)
b, Å	13.951(2)	13.860(2)	16.6501(10)	12.2511(6)	12.206(5)
c, Å	20.478(3)	20.390(4)	18.5674(12)	21.5922(11)	21.559(8)
α, deg	95.609(3)	95.552(3)	90	80.6240(10)	80.42(3)
β, deg	104.539(3)	103.892(3)	98.7750(10)	80.1890(10)	79.95(3)
γ, deg	108.063(3)	107.641(3)	90	61.5970(10)	61.61(3)
V, Å^3	3348.6(10)	3317.6(10)	6459.6(7)	2748.7(2)	2718(2)
Z	2	2	4	2	2
T, °C	−173(2)	−173(2)	−173(2)	−75(2)	−80(1)
no. ind reflns	16 261	15 974	15 975	13 584	3781
no. data	16 261	15 974	15 975	13 584	2258
restraints	4	0	7	6	35
params	939	913	907	999	581
R_1[a] [$I > 2\sigma(I)$]	0.0341	0.0334	0.0297	0.0269	0.182[c,d]
wR_2[a] [$I > 2\sigma(I)$]	0.0873	0.0871	0.0604	0.0664	0.184[c,e]
R_1[a] (all data)	0.0383	0.0362	0.0412	0.0327	0.210
wR_2[a] (all data)	0.0907	0.0890	0.0658	0.0699	0.196
GOF[b]	1.028	1.051	1.013	1.016	1.53
largest peak hole, e/Å^3	1.692–2.174	2.228–1.753	1.513–1.528	1.378–0.874	0.172–0.163 fm/Å^3

[a] $R_1 = \sum|F_o| - |F_c|/\sum|F_o|$; $wR_2 = [\sum w(F_o^2 - F_c^2)^2/\sum wF_o^4]^{1/2}$. Refinement on F_o^2 for all reflections (having $F_o^2 \geq -3\sigma(F_o^2)$). wR_2 and GOF based on F_o^2, R_1 based on F_o, with F_o set to zero for negative F_o^2. The observed criterion of $F_o^2 > 2\sigma(F_o^2)$ is used only for calculating R_1 and is not relevant to the choice of reflections for refinement. [b] GOF = $[\sum w(F_o^2 - F_c^2)^2/(n-p)]^{1/2}$ (n = number of data, p = number of parameters varied; $w = [\sigma^2F_o^2 + (0.0638P)^2]^{-1}$, where $P = [\max(F_o^2, 0) + 2F_c^2]/3$. [c] Outliers with $|F_o^2/F_c^2| > 2$ and $|F_c^2/F_o^2| > 2$ and $|(F_o^2 - F_c^2)|/\sigma F_o^2 > 6$ were rejected, [$I > 3\sigma(I)$]. [d] $R_w(F^2) = \{\sum[w(F_o^2 - F_c^2)^2]/\sum[w(F_o^2)^2]\}^{1/2}$. [e] $R(F^2) = \sum|F_o^2 - F_c^2|/\sum|F_o^2|$, [$I > 3\sigma(I)$].

H_2O, and NH_3.[13]However, we have yet to exploit the unique cooperative reactivity for carbonaceous substrates. We now report organometallic transformations derived from M^n-M^{n+2} complexes that feature bimetallic cooperation of the two-electron mixed valence core of $Ir_2^{0,II}(tfepma)_3Cl_2$. The complex possesses an electron-rich Ir^0 center adjacent to a coordinatively unsaturated Ir^{II} center, which can be readily functionalized with organic substrates. The synthetic, X-ray, and neutron diffraction, redox isomerization, and intramolecular C−H bond activation studies reported herein serve to further expand the scope of M^n-M^{n+2} chemistry.

Experimental Section

General Considerations. All manipulations were carried out in an N_2-filled glovebox or under an inert atmosphere provided by a Schlenk line unless otherwise noted. All solvents were reagent grade (Aldrich) or better and were dried and degassed by standard methods.[14]

Methods. NMR data were collected at the MIT Department of Chemistry Instrument Facility (DCIF) on a Varian Inova Unity 500 spectrometer. NMR solvents (C_6D_6, CD_3CN, THF-d_8) were purchased from Cambridge Isotope Laboratories and purified by standard procedures prior to use. ^{1}H NMR spectra (500 MHz) were referenced to the residual protio impurities of the given solvent; $^{31}P\{^1H\}$ NMR (202.5 MHz) spectra were referenced to an external 85% H_3PO_4 standard. All chemical shifts are reported in the standard δ notation in parts per million; positive chemical shifts are to higher frequency from the given reference. Infrared spectra were recorded on a Bio-Rad XPS 150 FT-IR spectrometer in a Perkin-Elmer liquid cell equipped with KBr windows. Elemental analyses were performed by Robertson Microlit Laboratories. $[Ir^I(COD)Cl]_2$ (Strem) and C_6H_5MgBr (1.0 M in THF, Aldrich) were used without further purification. Hydrogen gas (Grade 5.0, Airgas) was passed through a U-tube immersed in liquid nitrogen prior to its introduction into reaction vessels. C_6D_5MgBr[15] and $Ir_2^{0,II}(tfepma)_3Cl_2$[16,17] were synthesized according to published procedures.

X-ray Crystallographic Details. Single crystals were immersed in a drop of Paratone N oil on a clean microscope slide, affixed to either a glass fiber or a human hair coated in epoxy resin, and then cooled to either −75 (**4**-*syn*) or −173 °C (**2**, **2**-d_{10}, and **3**). The crystals were then mounted on a Siemens three-circle goniometer platform equipped with an APEX detector. A graphite monochromator was employed for wavelength selection of the Mo Kα radiation (λ = 0.71073 Å). The data were processed and refined using the program SAINT supplied by Siemens Industrial Automation Inc. Structures were solved by a Patterson heavy atom map and refined by standard difference Fourier techniques in the SHELXTL program suite (6.10 v., Sheldrick G. M., and Siemens Industrial Automation Inc., 2000). Disordered atoms in the $-CH_2CF_3$ groups were fixed at idealized bond lengths where necessary, and site occupancies were refined and refined anisotropically for those groups that were split evenly. Otherwise the minor components of unevenly split $-CH_2CF_3$ groups were refined isotropically. Hydrogen atoms were placed in calculated positions using the standard riding model and refined isotropically; all other atoms were refined anisotropically. Unit cell parameters, morphology, and solution statistics for complexes **2**−**4**-*syn* are summarized in Table 1. All thermal ellipsoid plots are drawn at the 50% probability level, with $-CH_2CF_3$ groups, −NMe groups, and solvents of crystallization omitted for clarity.

Neutron Diffraction. Neutron diffraction data were obtained at the Intense Pulsed Neutron Source (IPNS) at Argonne National Laboratory using the time-of-flight Laue single-crystal diffractometer (SCD).[18–20] At the IPNS, pulses of protons are accelerated

(13) Veige, A. S.; Nocera, D. G. *Chem. Commun.* **2004**, 1958–1959.
(14) Armarego, W. L. F.; Perrin, D. D. *Purification of Laboratory Chemicals*, 4th ed.; Butterworth-Heinmann: Oxford, 1996.
(15) Bianco, V. D.; Doronzo, S. *Inorg. Synth.* **1976**, *12*, 164–166.
(16) Heyduk, A. F.; Nocera, D. G. *J. Am. Chem. Soc.* **2000**, *122*, 9415–9426.
(17) Heyduk, A. F.; Nocera, D. G. *Chem. Commun.* **1999**, 1519–1520.
(18) Schultz, A. J.; Teller, R. G.; Williams, J. M.; Lukehart, C. M. *J. Am. Chem. Soc.* **1984**, *106*, 999–1003.

into a heavy-element target 30 times a second to produce pulses of neutrons by the spallation process. With two position-sensitive area detectors and a range of neutron wavelengths, a solid volume of reciprocal space is sampled with each stationary orientation of the sample and the detectors. The SCD has two ^{6}Li-glass scintillation position-sensitive area detectors, each with active areas of 15 × 15 cm^2 and a spatial resolution of <1.5 mm. One of the detectors is centered at a scattering angle of 75° and a crystal-to-detector distance of 23 cm, and the second detector is at 120° and 18 cm. A crystal of *syn*-$Ir_2^{II,II}(tfepma)_3(H)_4$ (**4**-*syn*), with approximate dimensions of 2 × 2 × 1 mm^3 and weighing 6.8 mg, was coated with fluorocarbon grease, wrapped in aluminum foil, and glued to an aluminum pin that was mounted on the cold stage of a closed-cycle helium refrigerator and cooled to −80(1) °C. Details of the data collection and analysis procedures have been published previously.[18–23] The GSAS software package was used for structural analysis.[24] Initial atomic positions were taken from the X-ray structure of **4**; structural refinement was then followed using the neutron diffraction data. Hydride ligands bound to iridium were clearly located by difference Fourier maps. However elevated temperatures were required to maintain crystallinity, the structure showed complexity from disordered $-CH_2CF_3$ groups, and the limited data restricted the solution to isotropic refinement of all atoms in the final refinement. Full experimental details can be found in the Supporting Information.

NMR Kinetics. Variable-temperature NMR kinetics studies were performed in C_6D_6, wherein a solution of complex **2** (or **2**-d_{10}) in C_6D_6 was prepared. The solution was then filtered and sealed in a J. Young NMR tube. Kinetic runs were carried out over the range 20–40 °C (calibrated temperatures 22.2, 31.8, and 41.5 °C) in 10 degree increments. Temperature calibration was carried out using 100% ethylene glycol by standard procedures (see Supporting Information). Spectra were recorded every 10 min for 200 min for each run. Relative concentrations of **2** and **3** (**2**-d_{10} and **3**-d_{10}) were assessed by integration over one of the −NMe resonances characteristic for each complex in C_6D_6 (2.60 and 2.48 ppm, respectively). The integral over both peaks was then set to 6H, and then each peak was integrated separately. In all cases, both the appearance of **3** and the decay of **2** (**3**-d_{10} and **2**-d_{10}) were fit to a single exponential with rate constants that agree within error.

Preparation of $Ir_2^{II,II}(tfepma)_3(\mu\text{-}C_6H_4)(C_6H_5)H$ (2). A 500 mg amount of $Ir_2^{0,II}(tfepma)_3Cl_2$ (0.261 mmol, 1 equiv) was dissolved in 5 mL of THF, and the solution was frozen. In a separate vial, 2.1 equiv of C_6H_5MgBr (548 μL, 1.0 M THF solution) was diluted with 1 mL of THF, and the solution was frozen. Immediately upon thawing, the Grignard was added to the iridium complex dropwise, affecting a color change to light yellow. The solvent was then immediately removed, and the residue triterated with pentane (3 × 2 mL), then taken up in Et_2O (5 mL), and filtered through a plug of Celite. The light yellow solution was concentrated to about 3 mL and placed in a freezer (−35 °C) overnight. The supernatant was decanted, and the resulting white solid was washed with 2 mL of pentane to give 359 mg (69%) of $Ir_2^{II,II}(tfepma)_3(\mu\text{-}C_6H_4)(C_6H_5)H$ (**2**) as a colorless powder. ^{1}H NMR (THF-d_8) δ/ppm: –13.72 (ddt, 244.8 Hz, 20.4 Hz, 10.2 Hz, 1 H, Ir-*H*), 2.13 (m, 1H, $-OCH_2CF_3$), 2.74 (t, 8.9 Hz, 3H, −N*Me*), 2.82 (t, 10.2 Hz, 3H, −N*Me*), 2.83 (t, 6.4 Hz, 3H, −N*Me*), 3.24 (m, 1H, $-OCH_2CF_3$), 3.85 – 5.21 (m, 22H, $-OCH_2CF_3$), 6.62 (t, 6.8 Hz, 1H, C-*H*), 6.67 (t, 6.4 Hz, 2H, C-*H*), 6.78 (t, 10.2 Hz, 1H, C-*H*), 6.83 (t, 10.2 Hz, 1H, C-*H*), 7.01 (t, 5.9 Hz, 1H, C-*H*), 7.64 (t, 6.8 Hz, 1H, C-*H*), 8.00 (t, 8.1 Hz, 2H, C-*H*). ^{31}P{^{1}H} NMR (THF-d_8) δ/ppm: 24.09 (ddd, 370.4 Hz, 74.1, 26.7 Hz), 34.90 (m), 39.56 (dddd, 68.1 Hz, 35.6 Hz, 20.7 Hz, 8.9 Hz, 1P), 62.24 (dddd, 367.4 Hz, 91.8 Hz, 20.7 Hz, 8.9 Hz, 1P), 104.14 (dddd, 269.6 Hz, 30.0 Hz, 17.8 Hz, 8.9 Hz), 120.48 (ddd, 269.6 Hz, 26.7 Hz, 20.7 Hz). In C_6D_6 a multiplet is observed at 2.35 ppm for **2**. These resonances arise from the methylene protons of one of the tfepma ligands. The multiplet arises from the $^3J_{H-F}$ splitting from the three fluorines of the CF_3 group and the $^3J_{H-P}$ from the phosphorus, and they are observed in pure samples of **2**. IR(CD_3CN) ν_{Ir-H}/cm^{-1}: 2069. Anal. Calc for $C_{39}H_{43}N_3O_{12}F_{36}P_6Ir_2$: C, 23.42; H, 2.17; N, 2.10. Found: C, 23.21; H, 2.07; N, 1.99. Crystals suitable for X-ray diffraction were grown from concentrated Et_2O solutions layered with pentane at −35 °C as colorless blocks.

Preparation of $Ir_2^{II,II}(tfepma)_3(\mu\text{-}C_6D_4)(C_6D_5)D$ (2-d_{10}). Preparation of **2**-d_{10} proceeded in a similar manner to that of complex **2**. A 220 mg amount of $Ir_2^{0,II}(tfepma)_3Cl_2$ (0.115 mmol, 1 equiv) was dissolved in 5 mL of THF, and the solution was frozen. In a separate vial, 2.1 equiv of freshly prepared C_6D_5MgBr (482 μL, 0.5 M THF solution) was diluted with 1 mL of THF and the solution was frozen. Immediately upon thawing the Grignard was added to the iridium complex dropwise, affecting a color change to light yellow. Workup proceeded as outlined for **2**, giving 209 mg (90%) of $Ir_2^{II,II}(tfepma)_3(\mu\text{-}C_6D_4)(C_6D_5)D$ (**2**-d_{10}) as a colorless solid. ^{1}H NMR (CD_3CN) δ/ppm: 2.56 (t, 6.4 Hz, 3H, −N*Me*), 2.58 (t, 9.8 Hz, 3H, −N*Me*), 2.78 (t, 9.8 Hz, 3H, −N*Me*), 3.28 (m, 1H, $-OCH_2CF_3$), 3.38 (m, 1H, $-OCH_2CF_3$), 4.3–4.9 (m, 20H, $-OCH_2CF_3$), 4.13 (m, 1H, $-OCH_2CF_3$), 5.306 (m, 1H, $-OCH_2CF_3$). ^{31}P{^{1}H} NMR (CD_3CN) δ/ppm: 26.29 (dddd, 318.0 Hz, 32.4 Hz, 21.5 Hz, 9.9 Hz), 31.84 (dddd, 924.5 Hz, 32.4 Hz, 26.1 Hz, 18.7 Hz), 56.50 (ddm, 318.0 Hz, 113.2 Hz), 65.10, (ddd, 113.2 Hz, 23.6 Hz, 9.9 Hz), 83.3 (dm, ∼200 Hz), 93.33 (dddd, 924.5 Hz, 195.4 Hz, 26.1 Hz, 21.1 Hz). ^{2}H NMR (CH_3CN) δ/ppm: −13.61 (dm, 37 Hz, Ir-*D*), 6.5–7.2 (bm, C-*D*), 7.4–8.1 (bm, C-*D*). IR(CD_3CN) ν_{Ir-D}/cm^{-1}: 1453. Anal. Calc for $C_{39}H_{33}D_{10}N_3O_{12}F_{36}P_6Ir_2$: C, 23.30; H, 2.66; N, 2.09. Found: C, 23.58; H, 2.29; N, 1.93.

Preparation of $Ir_2^{I,III}(tfepma)_3(\mu\text{-}C_6H_4)(C_6H_5)H$ (3). A 235 mg (0.118 mmol) amount of $Ir_2^{II,II}(tfepma)_3(\mu\text{-}C_6H_4)(C_6H_5)H$ was suspended in 3 mL of C_6H_6 in a thick-walled glass bomb to give a light yellow solution. The flask was then placed in an oil bath at 50 °C for 6 h, after which the oil bath was allowed to cool slowly. The solvent was decanted to afford 150 mg (64%) of $Ir_2^{I,III}(tfepma)_3(\mu\text{-}C_6H_4)(C_6H_5)H$ (**3**) as colorless single crystals. ^{1}H NMR (CD_3CN) δ/ppm: −9.79 (ddt, 233.3 Hz, 23.8 Hz, 6.4 Hz, 1H, Ir-*H*), 2.47 (t, 7.0 Hz, 3H, −N*Me*), 2.79 (t, 6.4 Hz, 3H, −N*Me*), 2.87 (t, 9.8 Hz, 3H, −N*Me*), 3.2–3.4 (m, 4H, $-OCH_2CF_3$), 3.75–4.01 (m, 2H, $-OCH_2CF_3$), 4.1–4.9 (ovm, 18H, $-OCH_2CF_3$), 6.75 (t, 6.4 Hz, 1H, C-*H*), 6.83–6.92 (m, 4H, C-*H*), 6.99 (t, 6.4 Hz, 1H, C-*H*), 7.20 (t, 6.4 Hz, 1H, C-*H*), 7.74 (bs, 2H, C-*H*). ^{31}P{^{1}H} NMR (CD_3CN) δ/ppm: 17.47 (m), 28.45 (dt, 833.3 Hz, 42.4 Hz), 87.0 (m), 90.64 (dt, 174.90 Hz, 32.39 Hz), 92.45 (dd, 213 Hz, 14.98 Hz), 97.19 (dm, 213 Hz). In C_6D_6 a multiplet is observed at 2.69 ppm for **3**. As in **2**, the multiplet arises from the $^3J_{H-F}$ splitting from the three fluorines of the CF_3 group and the $^3J_{H-P}$ from the phosphorus of one of the tfepma ligands. IR(CD_3CN) ν_{Ir-H}/cm^{-1}: 2023. Anal. Calc for $C_{39}H_{43}N_3O_{12}F_{36}P_6Ir_2$: C, 23.42; H, 2.17; N, 2.10. Found: C, 23.33; H, 2.08; N, 2.00. Crystals suitable for X-ray diffraction were picked from the recrystallized product as colorless blocks.

Preparation of $Ir_2^{I,III}(tfepma)_3(\mu\text{-}C_6D_4)(C_6D_5)D$ (3-d_{10}). Arylation with C_6D_5MgBr proceeded as in the preparation of **2**-d_{10}, using 328 mg of $Ir_2^{0,II}(tfepma)_3Cl_2$ (0.171 mmol) and 180 μL of C_6D_5MgBr (0.5 M THF solution, 2.1 equiv). The material was worked up as in **2**-d_{10} except that after filtration through Celite the Et_2O solution was allowed to stir at ambient temperature for 16 h, concentrated to 3 mL, and placed in a freezer at −35 °C overnight

(19) Schultz, A. J.; Carlin, R. L. *Acta Crystallogr. B* **1995**, *51*, 43–47.
(20) Schultz, A. J.; De Lurgio, P. M.; Hammonds, J. P.; Mikkelson, D. J.; Mikkelson, R. L.; Miller, M. E.; Naday, I.; Peterson, P. F.; Porter, R. R.; Worlton, T. G. *Physica B* **2006**, *385–386*, 1059–1061.
(21) Jacobson, R. A. *J. Appl. Phys.* **1986**, *19*, 283–286.
(22) Schultz, A. J. *Trans. Am. Crystallogr. Assoc.* **1987**, *23*, 61–69.
(23) Schultz, A. J.; Van Derveer, D. G.; Parker, D. W.; Baldwin, J. E. *Acta Crystallogr. C* **1990**, *46*, 276–279.
(24) Larson, A. C.; Von Dreele, R. B. General Structure Analysis System (GSAS); Los Alamos National Laboratory Report LAUR 86-748, **2004**.

to furnish 241 mg (70%) of **3**-d_{10} as a colorless solid. Complex **3**-d_{10} can also be prepared by gently heating solutions of **2**-d_{10} in an analogous manner to the procedure employed to give complex **3** from **2**. ^{1}H NMR (CD_3CN) δ/ppm: 2.38 (m, 1H, $-OCH_2CF_3$), 2.47 (t, 6.7 Hz, 3H, $-NMe$), 2.79 (t, 7.3 Hz, 3H, $-NMe$), 2.87 (t, 9.8 Hz, 3H, $-NMe$), 3.15–3.35 (ovm, 3H, $-OCH_2CF_3$), 3.75–4.02 (m, 2H, $-OCH_2CF_3$), 4.1–4.9 (ovm, 18H, $-OCH_2CF_3$). ^{2}H NMR (CH_3CN) δ/ppm: −9.70 (dm, 34 Hz, Ir-*D*), 6.5–7.5 (bm, C-*D*), 7.79 (bm, C-*D*). ^{31}P{^{1}H} NMR (CH_3CN) δ/ppm: 22.48 (m), 33.56 (ddd, 874.0 Hz, 173.7 Hz, 31.7 Hz), 91.5 (m), 95.57 (ddd, 874.0 Hz 173.7 Hz, 31.7 Hz), 97.57 (dd, 212.3 Hz, 16.5 Hz), 102.14 (ddd, 212.3 Hz, 31.7 Hz, 26.6 Hz). IR(CD_3CN) $\nu_{Ir\text{-}D}$/cm^{-1}: 1415. Anal. Calc for $C_{39}H_{33}D_{10}N_3O_{12}F_{36}P_6Ir_2$: C, 23.30; H, 2.66; N, 2.09. Found: C, 23.79; H, 2.09; N, 1.95.

Preparation of $Ir_2^{II,II}$(tfepma)$_3$(H)$_4$ (4). A 374 mg amount of $Ir_2^{0,II}$(tfepma)$_3Cl_2$ was dissolved in 4 mL of THF with stirring, and the solution was frozen. In a separate vial, 2.1 equiv of C_6H_5MgBr (410 μL, 1.0 M THF solution) was diluted with 1 mL of THF, and the solution was frozen. Reaction and workup proceeded as for complex **2**. The resulting Et_2O solution (5 mL) was loaded into a thick-walled glass bomb with a Teflon valve and the vessel attached to a high-vacuum line. The solution was freeze–pump–thawed (1×10^{-5} Torr) for three cycles followed by the introduction of 1 atm of hydrogen, which was passed through a U-tube immersed in liquid nitrogen prior to charging the reaction vessel. The reaction vessel was then sealed, shaken vigorously for 10 min, and allowed to stand overnight. A colorless precipitate formed and was dissolved by the addition of 2 mL Et_2O. The resulting solution was filtered and placed in a freezer (−35 °C) overnight to afford 170 mg (47%) of $Ir_2^{II,II}$(tfepma)$_3$(H)$_4$ (**4**) as a colorless solid. Dynamic behavior is evident in the ^{1}H NMR spectrum of **4**. Whereas complexes **2** and **3** exhibit sharp, well-defined, hydride and −NMe resonances, those of **4** in THF-d_8 are considerably broadened. Four −NMe resonances are observed at 2.59, 2.73, 2.86, and 2.90 ppm. These results indicated the presence of two products in solution. Integration reveals a 2:1 ratio for the peaks at 2.73 and 2.90 ppm. A 2:1 ratio is also identified for the resonances at 2.86 and 2.59 ppm. The two sets of peaks integrate in a 3:2 ratio, in favor of the peaks at 2.73 and 2.90 ppm. The hydride region also indicates multiple components with resonances at −11.51 and −11.64 ppm observed as broad singlets, and a resonance centered at −14.40 ppm as overlapping broad multiplets. Integration over all −NMe resonances and all hydrides gave a 9:4 ratio, as expected for the $Ir_2^{II,II}$(tfepma)$_3$(H)$_4$ formulation. Crystals suitable for X-ray diffraction were grown from a subsequent reaction following the same procedure as above except that the reaction mixture in Et_2O was allowed to stand for several days. Large colorless blocks of *syn*-$Ir_2^{II,II}$(tfepma)$_3$(H)$_4$ deposited from solution. These crystals cracked easily and crystallinity was lost at temperatures below −80 °C, necessitating data collection at elevated temperatures. Consequently significant disorder for the $-CH_2CF_3$ groups of the tfepma ligands is observed. The crystals not used for X-ray analysis were loaded into a J. Young resealable NMR tube, which was attached to a high-vacuum line. THF-d_8 was then vacuum transferred into the tube while immersed in liquid nitrogen. The tube was warmed until the THF thawed, and then it was immediately transferred into the magnetic field of an NMR spectrometer maintained at −80 °C. The ^{1}H NMR spectrum showed the presence of multiple species in solution and neither the hydride nor the −NMe resonances exhibited noticeable sharpening. ^{1}H NMR (THF-d_8, 20 °C) δ/ppm: −14.65−14.20 (ovm, 3.5H, Ir-*H*), −11.51 (bs, 2H, Ir-*H*), −11.64 (bs, 1.5H, Ir-*H*), 2.59 (b, 1.5H, −N*Me*), 2.70 (bs, 6H, −N*Me*), 2.86 (b, 3.9H, −N*Me*), 2.90 (t, 6.7 Hz, 3H, −N*Me*), 4.05 – 4.86 (ovm, 40H, $-OCH_2CF_3$). ^{1}H NMR (THF-d_8, −80 °C) δ/ppm: −14.35 (ovm, 3.5 H, Ir-*H*), −11.58 (bs, 1.4 H, Ir-*H*), −11.405 (bs, 2H, Ir-*H*), 2.55 (b, 1.5H, −N*Me*), 2.64 (bs, 6H, −N*Me*), 2.88 (b, 4H, −N*Me*), 3.02 (t, 6.7 Hz, 3H, −N*Me*), 4.05–4.90 (ovm, 40H, $-OCH_2CF_3$). ^{31}P{^{1}H} NMR (THF-d_8, −80 °C): 102.5 (m), 110.2 (m), 113.0 (m), 115.4 (m), 118.1 (m), 121.5 (m). IR (CD_3CN) ν_{Ir-H}/cm^{-1}: 2036 (sharp), 1966 (br shoulder). Anal. Calc for $C_{27}H_{37}N_3O_{12}F_{36}P_6Ir_2$: C, 17.53; H, 2.02; N, 2.27. Found: C, 17.64; H, 2.04; N, 2.18. **2** may also serve as a synthon of **4**, but the hydrogenation competes with isomerization of **2** to **3**. In the interest of maximizing the yield of **4**, the hydrogenation was initiated from freshly prepared solutions of **2**. Neutron diffraction experiments were performed at the IPNS at Argonne National Laboratories (*vide supra*) on large single crystals of **4** ($2 \times 2 \times 1$ mm^3; 6.8 mg). Hydride ligand fractional occupancies refine to a value of unity for each ligand, suggesting that the hydrides are not disordered over the bimetallic core in the solid state.

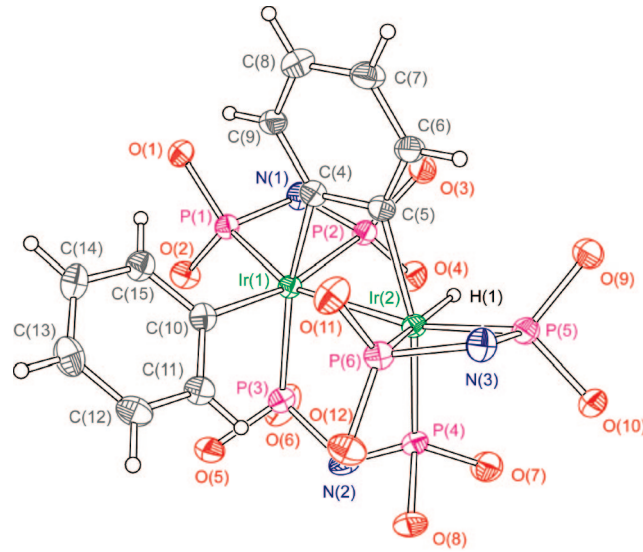

Figure 1. Solid state structure of $Ir_2^{II,II}$(tfepma)$_3$(μ-C_6H_4)(C_6H_5)H (**2**). Ellipsoids are drawn at the 50% probability level with −NMe and $-CH_2CF_3$ groups removed for clarity.

Results

Synthesis of $Ir_2^{II,II}$(tfepma)$_3$(μ-C_6H_4)(C_6H_5)H (2). The $Ir_2^{0,II}$(tfepma)$_3Cl_2$ (**1**) complex provides two convenient sites for functionalization via the halides of the Ir^{II} center. Indeed, aryl Grignard reagents react with **1** readily to effect the following conversion,

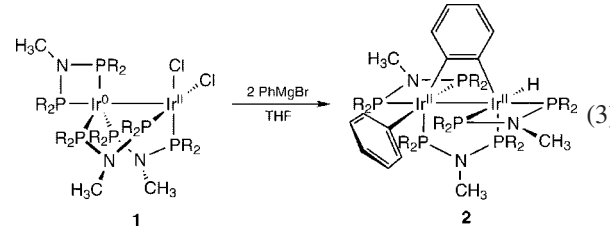

(3)

The identity of the reaction product **2** was revealed by single crystal X-ray diffraction analysis. The solid state structure of **2** is presented in Figure 1, and selected bond lengths and angles are listed in Table 2. The core of the complex is comprised of two octahedral Ir^{II} centers with an Ir−Ir bond distance of 2.7472(4) Å. The pseudo-octahedral geometry about each iridium center is similar, with a terminal phenyl and hydride distinguishing the coordination spheres of Ir(1) and Ir(2), respectively. The presence of a hydride ligand *trans* to P(6) is signified by a conspicuously vacant coordination site ($\angle$C(5)−Ir(2)−P(4) = 162.71(11)° and $\angle$P(5)−Ir(2)−Ir(1) = 166.95(3)°) in the early refinement cycles. The hydride was eventually located crystallographically but was

Table 2. Selected Bond Lengths and Angles for $Ir_2^{II,II}(tfepma)_3(\mu\text{-}C_6H_4)(C_6H_5)H$ (2)

Bond Lengths (Å)			
Ir(1)−Ir(2)	2.7472(4)	Ir(1)−P(2)	2.2770(10)
Ir(1)−C(4)	2.092(4)	Ir(1)−P(3)	2.2652(11)
Ir(1)−C(10)	2.125(4)	Ir(2)−P(4)	2.2532(10)
Ir(2)−C(5)	2.117(4)	Ir(2)−P(5)	2.2228(10)
Ir(1)−P(1)	2.2798(10)	Ir(2)−P(6)	2.3197(11)
Bond Angles (deg)			
P(5)−Ir(2)−Ir(1)	166.95(3)	P(1)−N(1)−P(2)	99.63(18)
C(5)−Ir(2)−P(4)	162.71(11)	P(1)−Ir(1)−P(2)	69.09(4)
C(4)−Ir(1)−Ir(2)	71.34(11)	P(3)−N(2)−P(4)	120.9(12)
C(5)−Ir(2)−Ir(1)	71.38(11)	P(5)−N(3)−P(6)	99.05(18)
P(2)−Ir(1)−C(10)	167.87(11)	P(5)−Ir(2)−P(6)	68.74(4)
Dihedral Angles (°)			
P(3)−Ir(1)−Ir(2)-P(4)	3.68(4)	C(4)−Ir(1)−Ir(2)-C(5)	2.54(16)

fixed at an idealized distance of 1.600 Å in later refinement cycles. The presence of one bridging and two chelating tfepma ligands represents the first occurrence of this motif for this ligand system; the more typical presentation of three tfepma ligands is for two to bridge the bimetallic core and one to chelate a single metal. The flexibility of the tfepma PNP backbone is indicated by the ligand's ability to accommodate both the tight bite angle required for chelation ($\angle$P(1)−N(1)−P(2) = 69.09(4)° and $\angle$P(5)−N(3)−P(6) = 68.74(4)°) and the expanded angle required for bridging a dinuclear core ($\angle$P(3)−N(2)−P(4) = 120.9(2)°). The most prominent structural feature of **2** is the μ-η^2-benzyne ligand that spans the diirdium core. Benzyne complexes are typically encountered when the ligand is bound to mononuclear metal centers of early and late metals[25,26] or higher nuclearity clusters composed of metals in low oxidation states.[27] The observation of benzyne groups bound to two metals is uncommon. Benzyne adsorbed on an Ir{100} surface appears to assume a μ-benzyne bonding mode.[28] At the molecular level, $[Ir_2(\mu\text{-o-}C_6H_4)(\eta^5\text{-}C_5H_5)_2(CO)_2]$,[29] $[Ir_2(\mu\text{-o-}C_6H_4)(\mu\text{-}PPh_2)(\mu\text{-}H)(\eta^5\text{-}C_5H_5)_2]$,[30] $[Ir_2(\mu\text{-}OH)(\mu\text{-}PAr_2)(\mu\text{-}C_6H_3R)(\eta^5\text{-}C_5Me_5)_2(CO)_2]$ (Ar = C_6H_5, *p*-$CH_3C_6H_4$ and R = H, CH_3),[31] and $[Fe_2(\mu\text{-o-}C_6H_4)(CO)_8]$[32] all present the benzyne in a bridge position with the C−C bond of the benzyne moiety parallel to the M−M axis. Recently a dipalladium complex [(dcpe)Pd(μ-o-C_6H_4)Pd-(dcpe)] was reported[33] in which the benzyne unit is twisted 46° from the Pd−Pd bond axis. In **2**, the C(4)−C(5) bond length of 1.405(5) Å is more closely akin to the distances observed in clusters as opposed to monomeric complexes. The benzyne may be viewed as an aromatic $C_6H_4^{2-}$ moiety in which two mutually *ortho* protons are substituted by iridiums from the bimetallic core. To compare, the Ir(1)−C(4) and Ir(2)−C(5) bond lengths of 2.092(4) and 2.117(4) Å, respectively, are similar and only marginally shorter than the sp^2-bound phenyl (Ir(1)−C(10) = 2.125(4) Å). The constrained four-atom ring created by the bridging benzyne and iridium atoms distorts the octahedral geometry of the $Ir_2^{II,II}$core (Ir(1): $\angle$C(15)−Ir(1)−Ir(2) = 71.5(2)°, Ir(2): $\angle$C(10)−Ir(2)−Ir(1) = 71.0(3)°) and the angles around the Ir−C atom connections (C(10): ($\angle$Ir(10)−C(10)−C(15) = 108.1(6)° and $\angle$C(11)−C(10)−Ir(2) = 131.6(7)°, C(15): $\angle$Ir(1)−C(15)−C(10) = 109.1(6)° and $\angle$C(14)−C(15)−Ir(1) = 131.6(7)°). Notably the Ir(2)−P(6) bond length of 2.3197(11) Å is markedly longer than the corresponding Ir(1)−P(2) bond length of 2.2770(10) Å, reflecting the significant *trans* influence of the hydride ligated to Ir(2). All other bond lengths and angles within the terminally bound and bridging aromatic rings are normal.

In solution, **2** retains its solid state structure. An ^{1}H NMR spectrum of **2** obtained in THF-d_8 reveals a hydride resonance at –13.73 ppm as an apparent doublet of doublet of triplets (ddt). Coupling of the hydride to its *trans* ($^2J_{P-H}$ = 244.8 Hz) and *cis* ($^2J_{P-H}$ = 20.4 Hz, 10.2 Hz) phosphorus neighbors is observed. The observed splitting pattern for this hydride suggests the involvement of an additional coupling, either a long-range J_{H-P} through the Ir−Ir bond or an additional coupling to a ^{31}P nucleus through the PNP ligand backbone. In either case, the hydride resonance for **2** should appear as a doublet of doublet of doublet of doublets (dddd); however the apparent ddt can be rationalized by similar coupling to two chemically distinct ^{31}P nuclei. The resonances for the −NMe groups on the diphosphazane ligand appear as three triplets at 2.74 ppm ($^3J_{P-H}$ = 8.9 Hz), 2.82 ppm ($^3J_{P-H}$ = 10.2 Hz), and 2.83 ppm ($^3J_{P-H}$ = 6.4 Hz). The doubly chelating and one bridging binding motif observed in the solid state for **2** allows for the assignment of the resonances at 2.74 and 2.83 ppm as those that chelate the iridium centers based on $^3J_{P-H}$ coupling constants. The observed coupling constants for the chelating tfepma ligands are larger than that of the bridging tfepma −NMe resonance by ~2 Hz. The trifluoroethoxy proton resonances present a characteristically complicated pattern of overlapping multiplets. The aryl region consists of seven well-defined resonances. The absence of line broadening in this region suggests that the coordinated phenyl group on Ir(1) is most likely freely rotating and is not locked into a single configuration due to steric congestion with the $-OCH_2CF_3$ groups of the tfepma ligand. Sharp resonances are to be expected for the bridging benzyne. Six distinct resonances are observed in the ^{31}P{^{1}H} NMR spectrum, which is well defined but complicated owing to the observation of $^2J_{P-P}$ *cis* couplings through the PNP ligand backbone and also for the chelating tfepma ligands through the iridium centers.

The deuterated product, **2**-d_{10}, is readily accessed using C_6D_5MgBr in place of C_6H_5MgBr. The solid state structure of **2**-d_{10} is completely analogous to **2** (see Tables 1 and S2.8). The presence of the hydride, although implicated by crystallographic studies and the ^{1}H NMR, is unambiguously shown with infrared spectroscopy. An Ir−H stretching frequency at 2069 cm^{-1} shifts to 1453 cm^{-1} upon deuteration; a simple Hooke's law calculation, assuming no change in force constants, predicts a shift to 1463 cm^{-1} for these stretches upon isotopic substitution of deuterium for hydrogen. Using the observed stretching frequencies, the deviations in Ir−H/D force constants upon isotopic substitution is estimated to be f_{Ir-H}/f_{Ir-D} = 1.02 for **2**.

Isomerization Chemistry. Although both the ^{1}H and ^{31}P{^{1}H} NMR of **2** indicate a static structure in solution, over time, room-temperature solutions of **2** slowly isomerize to furnish the $Ir_2^{I,III}(tfepma)_3(\mu\text{-}C_6H_4)(C_6H_5)H$ complex **3** in near quantitative yield. The progress of the isomerization can be monitored by ^{1}H NMR spectroscopy and is accelerated by gentle heating at 50 °C in C_6H_6 for 6 h. Analysis of the resulting colorless product

(25) Bennet, M. A.; Wenger, E. *Chem. Ber. Recl.* **1997**, *130*, 1029–1042.
(26) Jones, W. M.; Klosin, J. *Adv. Organomet. Chem.* **1998**, *42*, 147–221.
(27) Brait, S.; Deabate, S.; Knox, S. A. R.; Sappa, E. *J. Clust. Sci.* **2001**, *12*, 139–173.
(28) Johnson, K.; Sauerhammer, B.; Titmuss, S.; Hing, D. A. *J. Chem. Phys.* **2001**, *114*, 9539–9548.
(29) Rausch, M. D.; Gastinger, R. G.; Gardner, S. A.; Brown, R. K.; Wood, J. S. *J. Am. Chem. Soc.* **1977**, *99*, 7870–7876.
(30) Grushin, V. V.; Vymenits, A. B.; Yanovskii, A. I.; Struchkov, Y. T.; Vol'pin, M. E. *Organometallics* **1991**, *10*, 48–49.
(31) McGhee, W. D.; Foo, T.; Hollander, F. G.; Bergman, R. G. *J. Am. Chem. Soc.* **1988**, *110*, 8543–8545.
(32) Bennet, M. J.; Graham, W. A. G.; Stewart, R. P., Jr. Tuggle, R. M. *Inorg. Chem.* **1973**, *12*, 2944–2949.
(33) Retbøll, M.; Edwards, A. J.; Rae, A. D.; Willis, A. C.; Bennet, M. A.; Wenger, E. *J. Am. Chem. Soc.* **2002**, *124*, 8348–8360.

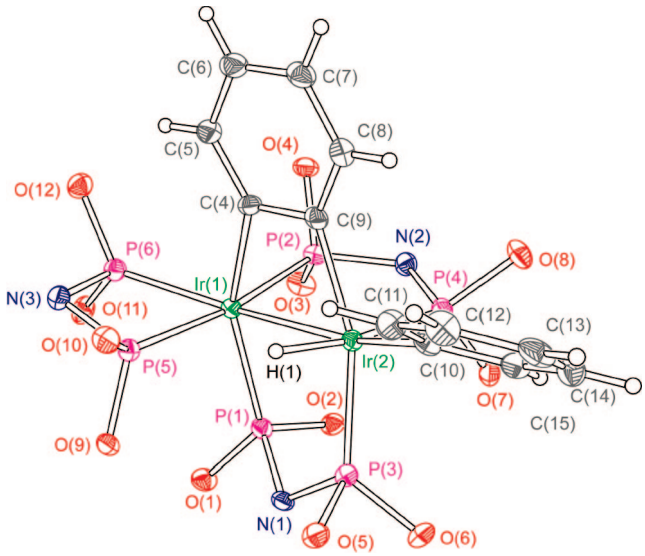

Figure 2. Solid state structure of $Ir_2^{I,III}(tfepma)_3(\mu\text{-}C_6H_4)(C_6H_5)H$ (**3**). Ellipsoids are drawn at the 50% probability level with −NMe and $-CH_2CF_3$ groups removed for clarity.

by ^1H NMR in CD_3CN reveals a complex with three −NMe resonances as sharp triplets at 2.47, 2.79, and 2.87 ppm. The resonances integrate in a 1:1:1 ratio and exhibit $^3J_{P-H}$ coupling constants of 7.0, 6.4, and 9.8 Hz, respectively. Examination of the coupling constants indicates that the tfepma ligands have rearranged from a doubly chelating and one bridging geometry as in **2** to a doubly bridging and one chelating motif as shown in eq 4,

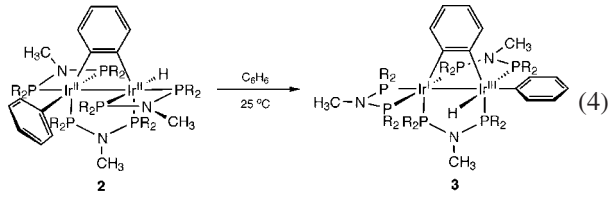

(4)

The hydride resonance at −9.79 ppm for **2** is shifted downfield considerably from −13.73 ppm for that in **3**, indicating that its chemical environment has been significantly altered. The aryl region of **3**, as in **2**, exhibits seven resonances, several of which overlap considerably. A broadened singlet resonance at 7.74 ppm indicates some degree of rotational freedom for the hydrogens on the phenyl ring. The $^{31}P\{^1H\}$ NMR spectrum of **3** displays six distinct resonances and exhibits complex splitting patterns resulting from multiple $^2J_{P-P}$ couplings similar to those of **2**.

The molecular structure of **3** is definitively identified by X-ray structural analysis, the results of which are shown in Figure 2. Selected bond lengths and angles are listed in Table 3. The Ir−Ir separation in **3** lengthens slightly to 2.7791(2) Å. Consistent with the $^3J_{P-H}$ coupling constants observed in the ^1H NMR, the more common ligation motif of two bridging and one chelating tfepma is found in complex **3**. The equatorial hydride is inferred by the open coordination site *trans* to P(4) (∠C(10)−Ir(2)−Ir(1) = 160.73(10)° and ∠C(9)−Ir(2)−P(3) = 160.98(9)°). The hydride was located late in the refinement and was fixed at a bond length of 1.600 Å. Infrared spectroscopy shows that the Ir−H stretching frequency shifts appropriately from 2023 to 1415 cm^{-1} upon isotopic substitution of deuterium for hydrogen (ν_{Ir-D}(calc) = 1426 cm^{-1}). Analogous to complexes **2** and **2**-d_{10}, the small deviation from calculated isotopic shifts implies a slightly reduced force constant (f_{Ir-H}/f_{Ir-D} = 1.03). The terminal phenyl resides along the Ir−Ir bond axis in an axial coordination site with a C(10)−Ir(2)−Ir(1) angle of 160.73(10)° and an Ir(2)−C(10) bond distance of 2.111(3) Å. Whereas the $C_6H_4^{2-}$ unit of the bridging benzyne maintains a nearly planar configuration with the diiridium core (C(4)−Ir(1)−Ir(2)−C(9) dihedral = 3.05(13)°), the terminal phenyl group is twisted by 57.85(30)° with respect to the plane comprised of the diiridium benzyne unit as measured by the C(9)−Ir(2)−C(10)−C(11) dihedral angle. Examination of the steric environments about the terminal phenyl group in the solid state reveals an expanded pocket relative to that observed for **2**, explaining the observation of slightly broadened resonances for the terminal phenyl protons in the ^1H NMR of **3**. The bridging benzyne distorts the octahedral geometries of the iridium centers. The angles within the four-atom bridge are significantly contracted (∠C(4)−Ir(1)−Ir(2) = 70.22(9)° and ∠C(9)−Ir(2)−Ir(1) = 71.83(10)°) and the iridium−carbon contacts are more asymmetric in **3** (d(Ir(1)−C(4)) = 2.141(3) Å and d(Ir(2)−C(9)) = 2.096(4) Å Δ(**3**) = 0.045 Å vs Δ(**2**) = 0.025 Å) than in **2**. The shortest contact observed for the benzyne carbons is that bonded to the Ir^{III} center. This is most likely due to the slightly contracted ionic radius of Ir^{III} vs Ir^{II}. The rearrangement of hydride and phenyl to terminal locations on the same iridium center represents a formal disproportionation of the valence symmetric $Ir_2^{II,II}$ core to a two-electron mixed valence $Ir_2^{I,III}$ core. The formal oxidation states and the Ir−Ir single bond in the two-electron mixed valence complex **3** are rationalized by a dative bonding interaction from a filled d_{z^2} orbital (taking the diiridium vector as the z axis) on the Ir^I center into an empty d_{z^2} orbital on the Ir^{III} center. This general bonding description has been described in detail for two-electron mixed valence $Rh_2^{0,II}$ dimers.[34]

Table 3. Selected Bond Lengths and Angles for $Ir_2^{I,III}(tfepma)_3(\mu\text{-}C_6H_4)(C_6H_5)H$ (3)

Bond Lengths (Å)			
Ir(1)−Ir(2)	2.7791(9)	Ir(1)−P(2)	2.2585(9)
Ir(1)−C(4)	2.141(5)	Ir(2)−P(3)	2.2225(10)
Ir(2)−C(9)	2.096(4)	Ir(2)−P(4)	2.2478(9)
Ir(2)−C(10)	2.111(3)	Ir(1)−P(5)	2.2585(9)
Ir(1)−P(1)	2.2793(10)	Ir(1)−P(6)	2.2878(9)
Bond Angles (deg)			
C(4)−Ir(1)−P(1)	151.82(10)	P(1)−Ir(1)−P(2)	93.42(3)
C(9)−Ir(2)−P(3)	160.98(9)	P(1)−N(1)−P(3)	115.37(17)
C(4)−Ir(1)−Ir(2)	70.22(9)	P(3)−Ir(2)−P(4)	102.53(3)
C(9)−Ir(2)−Ir(1)	71.83(10)	P(2)−N(2)−P(4)	121.44(17)
P(6)−Ir(1)−Ir(2)	157.30(2)	P(5)−N(3)−P(6)	98.81(15)
P(2)−Ir(1)−P(5)	171.56(4)	P(5)−Ir(1)−P(6)	68.46(3)
Dihedral Angles (deg)			
P(1)−Ir(1)−Ir(2)−P(3)	21.58(3)	C(4)−Ir(1)−Ir(2)−C(9)	3.05(13)
P(2)−Ir(1)−Ir(2)−P(4)	12.00(3)	C(9)−Ir(2)−C(10)−C(11)	57.85(30)

The rate of the **2** → **3** conversion was monitored by ^1H NMR spectroscopy. Although sparingly soluble, C_6D_6 was chosen for the reaction medium, as in this solvent the −NMe resonances exhibit little overlap. Mixtures of **2** and **3** display six well-defined triplets in this region between 1.97 and 2.60 ppm (Figure 3). The resonances at 1.97, 2.17, and 2.60 ppm are assigned to **2**, and the resonances at 2.02, 2.12, and 2.48 ppm to **3**. Examination of the isomerization end point shows no incorporation of the deuterium labels from the C_6D_6 solvent into the coordination sphere of **3**. Integration of the hydride and −NMe resonances at 2.60 ppm and 2.48 ppm, respectively, gives the expected ratio of 3:1 in the final product. Removal of all volatiles followed by addition of CD_3CN allows for

(34) Nocera, D. G. *Acc. Chem. Res.* **1995**, *28*, 209–217.

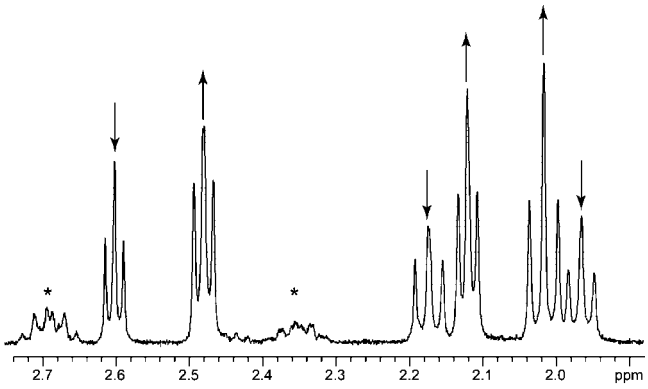

Figure 3. Segment of the ^{1}H NMR spectrum for a partially isomerized mixture of **2** and **3** in C_6D_6. The spectrum emphasizes the six triplet −NMe resonances, with arrows indicating the course of the spectral evolution with time. For the kinetic analysis, the resonances at 2.60 and 2.48 ppm were employed as signatures of **2** and **3**, respectively. Resonances indicated by a star are those of methylene protons on the $-OCH_2F_3$ groups of the tfepma ligands identified in pure samples of **2** and **3**.

Table 4. Observed Rate Constants and Calculated Activation Parameters for the Isomerization of 2 to 3 and 2-d_{10} to 3-d_{10}

	k_{obs} (s^{-1})		
	22.2 °C	31.8 °C	41.5 °C
2	2.94×10^{-5}	9.57×10^{-5}	3.09×10^{-4}
2-d_{10}	5.14×10^{-5}	2.17×10^{-4}	7.52×10^{-4}
	activation parameters		
	$\Delta H^{\ddagger}$ (kcal/mol)	$\Delta S^{\ddagger\ddagger}$ (eu)	
2	21.7 ± 0.3	−7.4 ± 0.9	
2-d_{10}	24.9 ± 0.7	−6.4 ± 2.4	

integration of the −NMe resonance at 2.87 ppm versus and the aryl region without interference from residual protio resonance from C_6D_6; the expected ratio of 3:9 is obtained. Additionally, no signals from intermediates are observed during the course of the reaction; the only observed NMe, aryl, or hydride resonances at any point in the reaction are assignable to either **2** or **3**.

The resonances of the bridging tfepma ligands at 2.60 and 2.48 ppm appear in an uncongested portion of the spectrum and consequently can be reliably integrated. The integrated intensities for the peaks at 2.60 and 2.48 ppm fit a first-order exponential decay and growth, respectively (Figure S6−S8). The observed rate constants, listed in Table 4, agree within experimental error. k_{obs} increases with increasing temperature, and a linear fit of $\ln(k_{obs}/T)$ vs $1000/T$ (Figure 4) yields the activation parameters shown in Table 4. The effects of isotopic substitution could be ascertained using complex **2**-d_{10}. The isomerization of **2**-d_{10} to **3**-d_{10} exhibits significant rate enhancement relative to its nondeuterated parent complex (Table 4). The observed rate constant of 2.17×10^{-4} s^{-1} at 31.8 °C in C_6D_6 solution yields an inverse isotope effect of k_{obs}^{H}/k_{obs}^{D} of 0.44 ± 0.1. As for **2**, the activation parameters were calculated from kinetic data measured over the range 20–40 °C and yielded a $\Delta H^{\ddagger}$ of 24.9 ± 0.7 kcal/mol and a $\Delta S^{\ddagger}$ of −6.4 ± 2.4 eu (Table 4). The inverse isotope effect is striking, as it indicates significant involvement of Ir−H(D)/C−H(D) bond making/breaking along the reaction coordinate. The isotope effect and the lack of observable intermediates over the course of the isomerization strongly indicate that the rate-determining step takes the form of an Ir−H(D)/C−H(D) bond making/breaking event, with any subsequent rearrangement steps leading to the formation of **3** occurring fast on the NMR time scale.

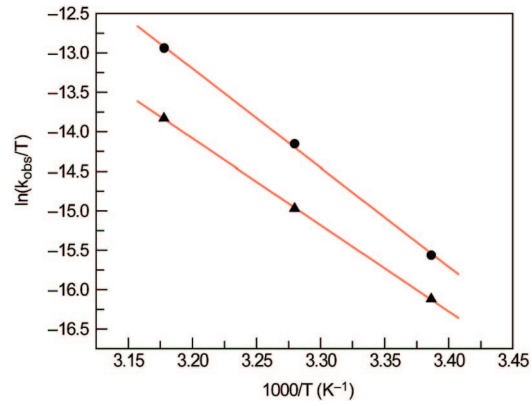

Figure 4. Plot of k_{obs} vs $1000/T$ for the isomerization of **2** to **3** (triangles) and **2**-d_{10} to **3**-d_{10} (circles) from which the activation parameters listed in Table 4 were extracted.

Whereas the iridium phenyl hydride functionality is dynamic in **2**, it is not in **3**. Even with the favorable *cis* coordination of a hydride and a phenyl group on the Ir^{III} center, no evidence for exchange of the terminal C_6H_5, benzyne C_6H_4, or hydride with solvent is observed after extended thermolysis in C_6D_6 at 70 °C (24–48 h) as assessed by ^{1}H NMR spectroscopy. At temperatures greater than 80 °C, only decomposition of the bimetallic core is observed.

Hydrogenation Chemistry. Observation of an inverse isotope effect for the isomerization of **2** and **2**-d_{10} implies the involvement of C−H(D) bonds in the transition state. Though the intermediacy of σ-C_6H_6 or η^2-π-C_6H_6 in the reductive elimination of benzene has been debated in the literature,[35,36] the simplest postulate for C−H(D) involvement in this report entails a reductive coupling of the benzyne and hydride on a single iridium center to generate an intermediate with either an open coordination site or a labile σ-C_6H_5 or η^2-π-C_6H_6 complex to a low-valent Ir^0 center as follows,

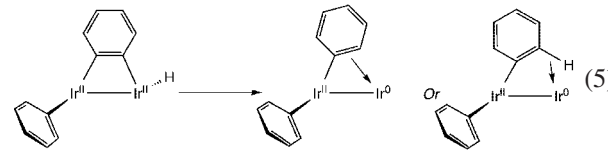

(5)

Under the canopy of this postulate, we sought to trap a coordinatively unsaturated intermediate. The use of a 10-fold excess of PMe_3 or ^{t}BuNC as a trapping reagent, however, gave multiple intractable products with overlapping resonances in the ^{1}H and ^{31}P{^{1}H} NMR. Hydrogen was chosen as a candidate since previous studies show that diiridium complexes related to **2** show a proclivity to readily activate hydrogen via vacant coordination sites.[10,11,16] We observed a smooth reaction of **2** with hydrogen to form the tetrahydride $Ir_2^{II,II}(tfepma)_3(H)_4$ (**4**) with concomitant formation of two benzene molecules (Scheme 1). The *syn* isomer was characterized by X-ray crystallography. A view along the Ir−Ir bond axis of **4**-*syn* is presented in Figure 5 and reveals a symmetric, triply bridged, tfepma core with the bridging ligands twisted ∼24° about the Ir−Ir bond axis. Selected bond lengths and angles are listed in Table 5. The core of complex **4**-*syn* is comprised of two octahedral iridium centers separated by 2.8389(3) Å with overall pseudo-C_{2v} symmetry.

(35) Johansson, L.; Tilset, M.; Labinger, J. A.; Bercaw, J. E. *J. Am. Chem. Soc.* **2000**, *122*, 10846–10855.
(36) Albéniz, A. C.; Schulte, G.; Crabtree, R. H. *Organometallics* **1992**, *11*, 242–249.

Scheme 1

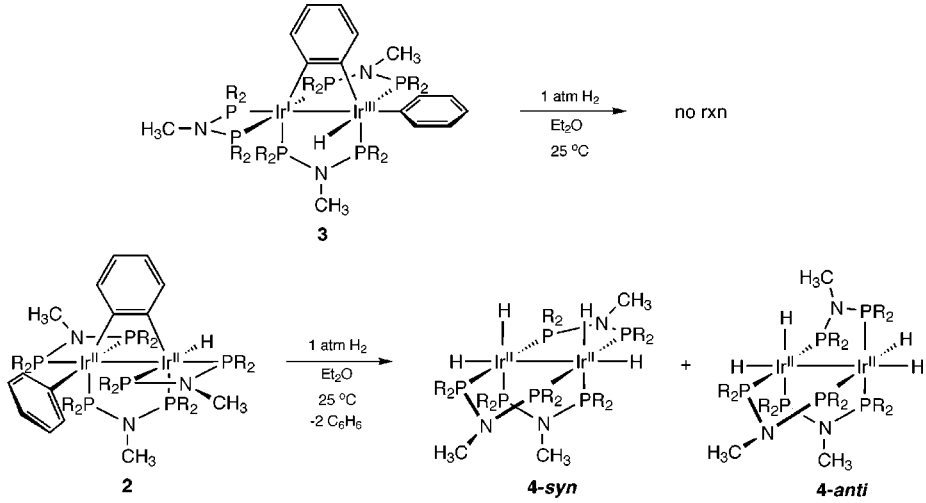

The elongated Ir−Ir bond (relative to **2** and **3**) most likely results from the absence of the bridging benzyne and to the presence of two strong *trans*-influencing terminal hydrides located in axial coordination sites relative to the metal−metal bond. Without the strained benzyne bridging unit, the geometry about the iridium centers is closer to that expected for an octahedron with *cis* phosphite angles in the range 95–99° (Table 5). Only a slight decrease in the *trans*-spanning phosphite angles are observed (∠P(1)−Ir(1)−P(3) = 165.13(3)° and ∠P(4)−Ir(2)−P(6) = 164.09(4)°) most likely due to the small hydride ligands in the equatorial positions.

The ^{1}H NMR of **4** reveals two sets of hydride resonances at −11.51 and −14.25 ppm tentatively assigned to the axially and equatorially bound (relative to the Ir−Ir internuclear axis) hydrides, respectively. Four broadened resonances at 2.59, 2.70, 2.86, and 2.90 ppm are observed in the region typical of a −NMe group. Integration over all the –NMe and hydride resonances gives a ratio of 9:4, as expected for the $Ir_2^{II,II}(tfepma)_3(H)_4$ formulation. Owing to the breadth of the hydride signals, variable-temperature NMR studies were conducted. Solutions prepared from single crystals of *syn*-$Ir_2^{II,II}(tfepma)_3(H)_4$ (**4**-*syn*) were placed in a resealable NMR tube, attached to a high-vacuum line, and THF-d_8 was vacuum-transferred into the tube while maintained at 77 K. The solution was then allowed to warm until the solvent thawed and then immediately placed into the magnetic field of an NMR spectrometer at −80 °C. Despite these precautionary measures, multiple products were observed and the band shape of the hydride resonances were not significantly sharpened. These results suggest that even at low temperatures the molecular structure of $Ir_2^{II,II}(tfepma)_3(H)_4$ is dynamic in solution but adopts a single conformation in the solid state. Based on results for related rhodium hydride complexes examined in our laboratories,[37] the dynamic behavior of **4** in solution is most likely due to a *syn* to *anti* isomerization, Scheme 1 bottom.

Though the hydrides of complex **4** could not be located reliably in the difference Fourier map obtained from X-ray diffraction, they were readily located using single-crystal neutron diffraction. Solution of the neutron diffraction data provides the structure presented in Figure 5 (right), consistent with that found by X-ray crystallographic techniques, except that the two pseudooctahedral iridium centers are completed by the presence of four crystallographically located terminal hydride ligands. The hydrides exhibit slightly compressed *cis* angles of 87.1(16)° and 81.0(16)° for the H(1)−Ir(1)−H(2) and H(3)−Ir(2)−H(4), respectively, and form nearly linear H−Ir−P angles with the *trans* phosphite on each iridium center (see Table 5). An acute H(2)−Ir(1)−Ir(2)−H(4) dihedral angle of 32.2(12)° confirms the *syn* disposition of the hydrides about the bimetallic core. The hydrides refine at full occupancy and disfavor the participa-

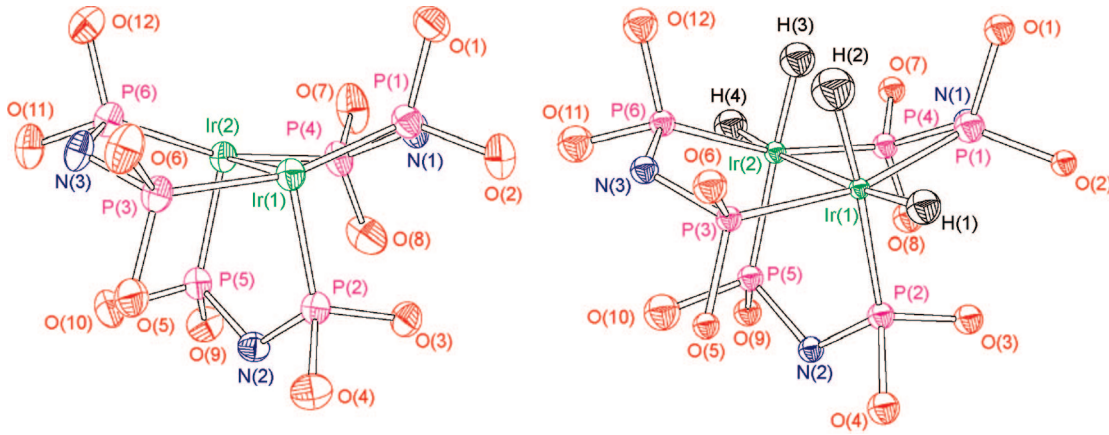

Figure 5. Single-crystal structure determinations for $Ir_2^{II,II}(tfepma)_3(H)_4$ (**4**) by X-ray (left) and neutron (right) diffraction methods. The neutron data unambiguously reveal the presence of four terminal hydrides ligated in a *syn* disposition over the bimetallic core of **4**. −NMe, $-CH_2CF_3$ groups are omitted for clarity, with thermal ellipsoids drawn at the 50% probability level. Displacement parameters were isotropically refined in the neutron structure, with ellipsoids drawn at the 50% probability level.

Table 5. Selected Bond Lengths and Angles for *syn*-$Ir_2^{II,II}(tfepma)_3(H)_4$ (4-*syn*) obtained from X-ray and Neutron Diffraction Methods

	X-ray	neutron		X-ray	neutron
		Bond Lengths (Å)[a]			
Ir(1)−Ir(2)	2.8389(2)	2.816(11)	Ir(2)−P(6)	2.2323(9)	2.242(19)
Ir(1)−P(1)	2.2420(9)	2.278(21)	Ir(1)−H(1)		1.636(30)
Ir(1)−P(2)	2.2514(9)	2.242(22)	Ir(1)−H(2)		1.647(33)
Ir(1)−P(3)	2.2263(8)	2.213(20)	Ir(2)−H(3)		1.599(30)
Ir(2)−P(4)	2.2223(9)	2.255(25)	Ir(2)−H(4)		1.612(32)
Ir(2)−P(5)	2.2467(9)	2.193(23)			
		Bond Angles (deg)[a]			
P(1)−Ir(1)−P(3)	165.13(3)	165.4(9)	P(5)−Ir(2)−P(6)	95.66(3)	96.6(8)
P(1)−Ir(1)−P(2)	97.02(3)	97.1(8)	H(1)−Ir(1)−H(2)		87.0(16)
P(2)−Ir(1)−P(3)	97.50(3)	97.1(8)	H(2)−Ir(1)−P(2)		174.4(12)
P(4)−Ir(2)−P(6)	165.09(4)	163.0(9)	H(3)−Ir(1)−H(4)		81.0(16)
P(4)−Ir(2)−P(5)	99.84(3)	99.9(9)	H(4)−Ir(1)−P(5)		175.5(13)
		Dihedral Angles (deg)[a]			
P(1)−Ir(1)−Ir(2)–P(4)	23.01(4)	22.5(7)	P(3)−Ir(1)−Ir(2)–P(6)	23.95(4)	24.0(7)
P(2)−Ir(1)−Ir(2)–P(5)	25.74(4)	26.1(7)	H(2)−Ir(1)−Ir(2)–H(4)		32.2(12)

[a] The hydride nomenclature in the table, H(1), H(2), H(3), and H(4), corresponds to H(b), H(c), H(d), and H(a), respectively, in the cif file.

tion of site disordered hydrides bridging the diiridium core in the solid state. Although dynamic in solution, the hydrides of **4** are resistant to exchange. Solutions of **4** in THF-d_8 when exposed to 1 atm of deuterium show no incorporation of label and maintain a static integral ratio of −NMe to hydride in the ^{1}H NMR spectrum after 1 week.

Unlike **2**, **3** did not react with hydrogen, and the complex decomposed after days at elevated temperatures (80–100 °C, Scheme 1). This observation is consistent with the stability of **3** and suggests that a coordinatively unsaturated intermediate cannot be attained with hydride in an equatorial position *cis* to both the benzyne and terminal phenyl ligands.

Discussion

Bimetallic cooperativity at two-electron mixed valence cores promotes the activation of C−H bonds. The bimetallic core of **1** provides a source of a "masked", electron-rich Ir^0 center adjacent to a coordinatively unsaturated Ir^{II} center. Because the bimetallic core is unsaturated, it is able to accept ligands into the bridging position and maintain a two-electron redox asymmetry. The formation of the benzyne complex subsequent to arylation is extremely fast and cannot be observed on NMR time scales. The subsequent isomerization of the kinetic product **2**, to its thermodynamic product, **3**, however occurs over hours at room temperature. This isomerization is enabled by cooperation of the diiridium centers, as there is no evidence that C_6H_6 is released from the bimetallic core followed by its readdition to the reduced metal center.

An inverse isotope effect for the isomerization rates of **2** and **2**-d_{10} in C_6D_6 implicates the involvement of C−H(D) bond forming/breaking reactions in the rate-determining step. Inverse isotope effects have been observed for the reductive coupling of alkyl hydrides[38–50] and less commonly aryl hydrides.[49–52] Inverse isotope effects are generally attributed to inverse

Scheme 2

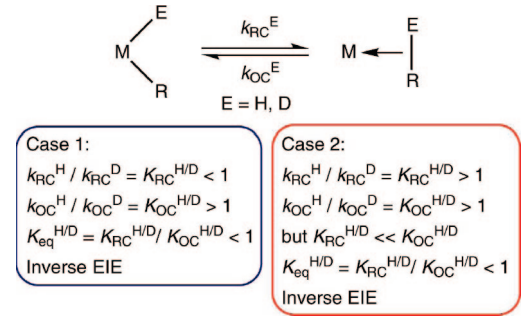

equilibrium effect as opposed to inverse kinetic isotope effect (i.e., $K_{H/D} < 1$[53] and not $k_H/k_D < 1$). Within this context, two distinct cases may give rise to an inverse isotope effect for the isomerization of **2** to **3**.[46,47] In the first case (Scheme 2, left) partial formation or breakage of the C−H(D) bond reduces the force constant relative to free C−H(D), and thus the ZPE (zero-point energy) for this intermediate species is presumed to fall between that of free C−H(D) and M−H(D). If this species is implicated in the transition state of the rate-determining step, then the differences in ZPE should engender a slight energetic preference (in the form of $\Delta G^{\ddagger}$) for reductive coupling in the deuterated complex. This thermodynamic preference would result in rate enhancement for this step, i.e., $k_{RC}^{H}/k_{RC}^{D} < 1$.

(37) Esswein, A. J.; Veige, A. S. ; Nocera, D. G. *J. Am. Chem. Soc.* **2005**, *127*, 16641–16651.
(38) Buchanan, J. M.; Stryker, J. M.; Bergman, R. G. *J. Am. Chem. Soc.* **1986**, *108*, 1537–1550.
(39) Periana, R. A.; Bergman, R. G. *J. Am. Chem. Soc.* **1986**, *108*, 7332–7346.
(40) Bullock, M. R.; Headford, C. E. L.; Hennessy, K. M.; Kegley, S. E.; Norton, J. R. *J. Am. Chem. Soc.* **1989**, *111*, 3897–3908.
(41) Parkin, G.; Bercaw, J. E. *Organometallics* **1989**, *8*, 1172–1179.
(42) Gould, G. L.; Heinekey, D. M. *J. Am. Chem. Soc.* **1989**, *111*, 5502–5504.
(43) Wang, C.; Ziller, J. W.; Flood, T. C. *J. Am. Chem. Soc.* **1995**, *117*, 1647–1648.
(44) Stahl, S. S.; Labinger, J. A.; Bercaw, J. E. *J. Am. Chem. Soc.* **1996**, *118*, 5961–5976.
(45) Wick, D. G.; Reynolds, K. A.; Jones, W. D. *J. Am. Chem. Soc.* **1999**, *121*, 3964–3983.
(46) Northcutt, T. O.; Wick, D. G.; Vetter, A. J.; Jones, W. D. *J. Am. Chem. Soc.* **2001**, *123*, 7257–7270.
(47) Lo, C. H.; Haskel, A.; Kapon, M.; Keinan, E. *J. Am. Chem. Soc.* **2002**, *124*, 3226–3228.
(48) Iron, M. A.; Lo, C. H.; Martin, J. M. L.; Keinan, E *J. Am. Chem. Soc.* **2002**, *124*, 7041–7054. Although the explanations for the observed isotope effects have been recently disputed in the literature, see refs 49 and 50.
(49) Churchill, D. G.; Janak, K. E.; Wittenburg, J. S.; Parkin, G. *J. Am. Chem. Soc.* **2003**, *125*, 1403–1420.
(50) Jones, W. D. *Acc. Chem. Res.* **2003**, *36*, 140–146.
(51) Jones, W. D.; Feher, F. J. *J. Am. Chem. Soc.* **1986**, *108*, 4814–4819.
(52) Watson, W. H.; Wu, G.; Richmond, M. G. *Organometallics* **2006**, *25*, 930–945.
(53) The equilibrium isotope effect $K_{eq}^{H/D}$ can be expressed as:

$$K_{eq}^{H/D} = \frac{k_{RC}^{H}/k_{OC}^{H}}{k_{RC}^{D}/k_{OC}^{D}} = \frac{k_{RC}^{H}/k_{RC}^{D}}{k_{OC}^{H}/k_{OC}^{D}}$$

Scheme 3

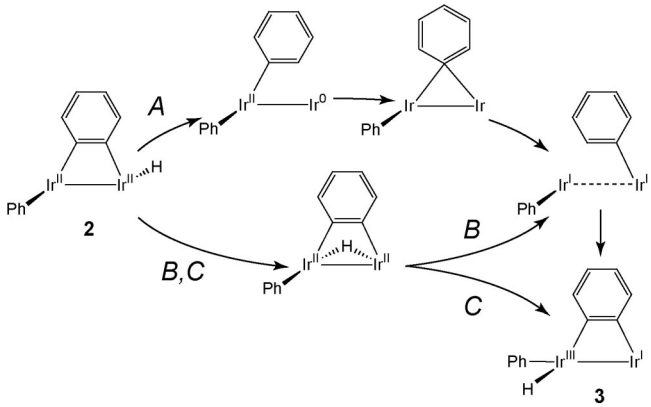

The microscopic reverse, oxidative cleavage, would be initiated from the σ-alkane product, which possesses intact C−H(D) bonds. Applying the same ZPE arguments as for the reductive coupling step would suggest a slight energetic preference for the protio case and, thus, a normal isotope effect, i.e., $k_{OC}{}^{H}/k_{OC}{}^{D} > 1$. Taking a combination of these rate constants gives an overall inverse equilibrium isotope effect. Alternatively, the C−H(D) stretching frequency is assumed to disappear as it becomes the reaction coordinate for the bond scission/formation. In this case (Scheme 2, right), normal kinetic isotope effects are expected for both the reductive coupling of the alkyl hydride and the oxidative cleavage of the resulting σ-alkane complex. The inverse isotope effect for the overall transformation arises due to the juxtaposition of the two normal kinetic isotope effects for the individual steps. In particular, when the magnitude of the normal kinetic isotope effect for oxidative cleavage of the σ-alkane complex is greater than that for the reductive coupling, an overall inverse isotope effect results. In general it is difficult to determine quantitatively whether the observed inverse isotope effect results from of a true inverse kinetic isotope effect or an inverse equilibrium isotope effect arising from two normal kinetic isotope effects.[46,50]

More phenomenologically, the observation of an inverse isotope effect for alkyl hydride complexes has become a standard measure for the intermediacy of σ-alkane complexes[50] and some arene complexes.[49,51] A complication for the latter is that the precise nature of the reductive coupling product is more ambiguous as both arene σ-C–H interactions (agostic type) and an η^2-π-arene interactions are possible as opposed to alkyl hydrides, where only an agostic C−H σ-alkane complex is a tenable intermediate.

Along these lines, the observation of an inverse isotope effect on the isomerization from **2** to **3** vs **2**-d_{10} to **3**-d_{10} likely implicates an intermediate with σ-C_6H_5 or η^2-π-C_6H_6 character resulting from reductive coupling along the reaction coordinate. Three reasonable pathways for the isomerization are shown in Scheme 3. Along path B, the reaction is initiated with the migration of the hydride to bridge the bimetallic core. The hydride then reductively couples with the benzyne at the adjacent iridium center to generate a valence symmetric $d^8 \cdots d^8$ diiridium core each ligated by a terminal phenyl group. Oxidative cleavage of an *ortho* C−H(D) bond will generate the two-electron mixed valence $Ir_2^{I,III}$ center of **3**. We note that this pathway is an intramolecular analogue of dinuclear elimination (eq 1) and is operative for H_2 addition and generation (eq 2) at two-electron mixed-valence cores. Alternatively, path A in Scheme 3 begins with reductive coupling of the hydride and benzyne, generating a two-electron mixed valence $Ir_2^{0,II}$ core. The reductive coupling reaction could be facilitated by prior dissociation of one arm of a tfepma ligand to generate a five-coordinate intermediate, as has been postulated for reductive elimination from a variety of Pt^{IV} complexes,[54–57] followed by phenyl migration through an μ-η^1-C_6H_5 intermediate.[58–62] Subsequent relaxation from μ-η^1-C_6H_5 to η^1-C_6H_5 unifies the two pathways via a common intermediate. From this intermediate, C−H(D) oxidative cleavage at the Ir^I center would generate the observed product **3**. A third mechanistic possibility (C) involving initial formation of a valence symmetric $Ir_2^{II,II}$ bridging hydride followed by valence disproportionation to an $Ir_2^{I,III}$ core without a C−H(D) bond formation/cleavage event is thought to be less likely than mechanisms A or B proposed in Scheme 3. The rationale begins by noting that a bridging hydride should have a lower force constant than a terminal hydride. This means that the ΔΔZPE difference between a terminal hydride/deuteride and a bridging hydride/deuteride transition state would be very small. Following the same logical progression as applied previously suggests that this small ΔΔZPE would result in smaller energetic preferences for either the protio or deutero congeners relative to the ΔΔZPEs for terminal M−H(D) and C−H(D) bonds. This means that the effects of isotopic substitution on a bridging hydride transition state should be small. The inverse isotope effect observed in this reaction however is large, ca. ∼0.44, suggesting that the transition states separating **2** from **3** or **2**-d_{10} from **3**-d_{10} confront significant energetic preferences resulting from isotopic substitution. This scenario is more consistent with C−H(D) bond cleavage/formation events along the reaction coordinate.[63] Unfortunately, the two favored pathways, A and B, are kinetically indistinguishable in the present study as **2** converted smoothly to **3** without the observation of any intermediates. Notwithstanding, either pathway relies on the cooperation of the valence asymmetric centers of the bimetallic core.

In summary, we have demonstrated that *ortho* C−H bond activation of coordinated phenyl groups across the metal−metal bond in two-electron mixed valent $Ir_2^{0,II}$ cores is facile. The primary C−H bond activation product, **2**, is a kinetic product, which undergoes a room-temperature redox isomerization to form the $Ir_2^{I,III}$ core of **3** as the thermodynamic product. The rate-determining step is implicated to involve C−H bond making/breaking step(s) on the basis of the observed inverse isotope effects and empirically by the interception of a reaction intermediate by hydrogen to give the tetrahydride species **4**. The kinetic data collected thus far, however, do not allow for the inverse isotope effect to be assigned as an inverse equilibrium isotope effect or a true inverse kinetic isotope effect for a single step (i.e., determination between case 1 and case 2 in Scheme 2), though to our knowledge, this report constitutes the first example of an inverse isotope effect involving C−H bonds

(54) Crumpton, D. M.; Goldberg, K. I. *J. Am. Chem. Soc.* **2000**, *122*, 962–963.
(55) Fekl, U.; Goldberg, K. I. *J. Am. Chem. Soc.* **2002**, *124*, 6804–6805.
(56) Jensen, M. P.; Wick, D. D.; Reinartz, S.; White, P. S.; Templeton, J. L.; Goldberg, K. I. *J. Am. Chem. Soc.* **2003**, *125*, 8614–8624.
(57) Crumpton-Bregel, D. M.; Goldberg, K. I. *J. Am. Chem. Soc.* **2003**, *125*, 9442–9456.
(58) Evans, D. G.; Hughes, G. R.; Mingos, D. M. P.; Bassett, J. M.; Welch, A. J. *J. Chem. Soc., Chem. Commun.* **1980**, 1255–1257.
(59) Nobel, D.; van Koten, G.; Spek, A. L. *Angew. Chem., Int. Ed. Engl.* **1989**, *28*, 208–210.
(60) Meyer, E. M.; Gamborotta, S.; Floriani, C.; Chiesi-Villa, A.; Guastini, C. *Organometallics* **1989**, *8*, 1067–1079.
(61) Bradford, C. W.; Nyholm, R. S.; Gainsford, G. J.; Guss, J. M.; Ireland, P. R.; Mason, R. *J. Chem. Soc., Chem. Commun.* **1972**, 87–89.
(62) Hlavinka, M. L.; Hagadorn, J. R. *Organometallics* **2005**, *24*, 5335–5341.
(63) We thank a reviewer for prompting this clarification.

measured in a bimetallic system. Finally, the results reported herein are noteworthy inasmuch as two-electron mixed valency at bimetallic cores tends to render complexes inert. Bosnich postulates[1–3] in his studies of binucleating complexes that bimetallic cores supported with a rigid ligand framework arrest multielectron redox reactivity of mixed-valence complexes. By employing a flexible ligand framework that permits the electronic and steric asymmetry of "multielectron" mixed valence cores to be accommodated, C−H activation pathways that are generally the purview of monometallic complexes become available at bimetallic centers working in concert.

Acknowledgment. A.J.E. would like to thank Prof. Joseph Sadighi and Prof. Theodore Betley for many helpful discussions. This work was supported under grants from the National Science Foundation (CHE-0450058). This work made use of the Shared Experimental Facilities (for single-crystal X-ray diffraction experiments) supported by the MRSEC Program of the National Science Foundation under award number DMR 02-13282, and the Department of Chemistry Instrument Facility (DCIF) at MIT for NMR data collection supported by the National Science Foundation under award number CHE-9808061 and DBI-9729592. Work at Argonne National Laboratory was supported by the U.S. Department of Energy, Office of Science, Office of Basic Energy Sciences, under contract DE-AC02-06CH11357.

Supporting Information Available: Kinetic data for the isomerization of **2** to **3** and **2**-d_{10} to **3**-d_{10}, NMR probe temperature calibration, thermal ellipsoid plots, tables of crystal data, atomic coordinates, bond lengths and angles, anisotropic thermal parameters, and hydrogen coordinates for complexes **2**, **2**-d_{10}, **3**, and **4**-*syn* are available in CIF format free of charge via the Internet at http://pubs.acs.org.

OM7007748